Int. J. Heat Mass Transfer. Vol. 33, No. 9, pp. 1987–1999, 1990
Printed in Great Britain

0017-9310/90 $3.00 + 0.00

Laminar forced convection from surface-mounted ribs

SHOU-SHING HSIEH,† HUEI-JAN SHIH and YING-JONG HONG
Department of Mechanical Engineering, National Sun Yat-Sen University, Kaohsiung, Taiwan 80424, Republic of China

(*Received* 12 *December* 1988 *and in final form* 16 *November* 1989)

Abstract—A study for both numerical and experimental aspects on low speed forced convective heat transfer near two-dimensional transverse ribs in which the walls are held at a uniform temperature is presented. The effects of aspect ratio and Reynolds number as well as the initial boundary layer thickness are examined and discussed. The numerical technique is based on a power law combined with a false stream function–vorticity form. It is found that the temperature data agree reasonably well with those taken from the experiments qualitatively. The results are further correlated by an equation of the form

$$\overline{Nu}_{s} = 0.44(Re_{s})^{0.465}(d/s)^{-0.3h}(w/s)^{-0.265}.$$

INTRODUCTION

THIS PAPER is concerned with numerical computations of a type of separated and reattached flow that is associated with the plane laminar flow over surface-mounted ribs. Such a flow field is complicated because two and possibly three separated regions exist. The first region starts from the upstream wall near the rib and reattaches on the front wall of the rib, which is often located below that corner; the second region separates from the rear wall and reattaches on the downstream wall. A third recirculating region attached to the top of the rib may exist if the rib is long enough. After the last region, the flow reattaches, the boundary layer redevelops, and the flow is laminar thereafter. Furthermore, the pressure gradient across the rib is extremely large and the Nusselt number increases rapidly to a high value. The objective of the present study is therefore to explore the details of the heat transfer characteristics in the vicinity of the rib including the separated and reattached flow region. The work is motivated from a recent development in the cooling of electronic equipment and gas cooled reactors as well as in high performance heat exchangers where more quantitative information on heat transfer rates in separated/reattached flow regions is needed. See, for example, Buller and Kilburn [1], Wirtz and Dykshoorn [2], and Hsieh [3]. There are very few studies on this topic in the literature, especially for the laminar case. More recently, Hsieh and Huang [4], and the subsequent work, Hsieh and Huang [5], computed the laminar flow field over an isolated rib using the finite-difference formulation for u, v, p, T. The rapid change in pressure and the heat transfer characteristic were reported. The pressure was found to drop rapidly immediately downstream of the rib followed by a steady recovery. The heat transfer coefficients were obtained for a rib aspect ratio (width/height) of $w/s = 1$, 2, and 4 at different Reynolds numbers covering the range $63.5 < Re_{s} < 254$. Details of the flow field and heat transfer characteristics such as pressure distribution across the rib and the separated and reattached length as well as heat transfer rates are not presented in Hsieh and Huang [4, 5]. Especially, the effect of the approaching boundary layer thickness was not reported.

In the present study, the fully laminar situation in which not only the flow approaching the rib is laminar, but the flow in both separated as well as in the reattached, redeveloping boundary layers is laminar. In addition, the plate upstream of the rib is considered to have a finite length so that the boundary layer thickness at the rib becomes a parameter that must be reckoned with. Aung [6] presented heat transfer measurements for laminar flow past backsteps where the stepwalls are maintained at a constant temperature. Results are given for the local heat transfer distributions as well as the average value for all the rib surfaces. It was found that in Aung [6] the average Stanton number exhibits a minus one-half power dependency on the Reynolds number. This relationship is in agreement with the wall independent, thin shear-layer analysis originally formulated for high speed, laminar flow with vanishing initial shear-layer thickness reported by Chapman [7]. Since the wall-independent shear layer analysis at least in one case has been successful in precisely predicting the experimental data, it is of interest to examine further the fundamental properties of the analysis of separated flow on the rib, and to observe how they relate to each other.

In addition to the above, it is also noted that the experimental results have not provided a satisfactory explanation regarding the role of the initial shear layer

† Author to whom correspondence should be addressed.

NOMENCLATURE

d	boundary layer thickness at the location of the rib computed in its absence (equation (6)) [cm]
H	height of top boundary [cm]
L_D	length of downstream boundary [cm]
n	normal to rib surface
$\overline{Nu}_{av}$	average Nusselt number, $h \cdot s/k$
p_0	freestream pressure [N m^{-2}]
$\bar{p}$	dimensionless pressure, $(p-p_0)/\rho U_0^2$
Re_s	Reynolds number based on rib depth
s	rib depth [cm]
T_0	freestream temperature [°C]
T_w	wall temperature [°C]
U_0	freestream velocity [m s^{-1}]
u, v	velocity in the x- and y-directions, respectively [m s^{-1}]
w	rib width [cm]
x_0	distance of leading edge from the rib [cm].

Greek symbols

α	ratio of two adjacent grid sizes (= 1.239)
β	maximum residual
θ	dimensionless temperature
ρ	density [kg m^{-3}]
ψ	stream function
ω	dimensionless vorticity.

Subscripts

D	distance
s	rib depth.

in separated forced convection. The results obtained from Aung [6] indicate a relatively strong effect of the initial shear-layer thickness on the average heat transfer for a backward facing step. By contrast, Bhatti and Aung [8] reported that the shear-layer thickness has a rather wild influence on the average heat transfer in the case of laminar flow past cavities. The heat transfer in separated forced convection is mainly effected through a vortex flow mechanism. Moreover, for flow over the surface-mounted ribs, it appears that there has been no report of such a study in the open literature. Therefore, it is worthwhile to examine how the strength of vortices in the separated flow region depends on the initial boundary-layer thickness and other related parameters for flow over surface-mounted ribs.

In the present computation, the finite-difference scheme using a false transient stream function–vorticity function is adopted. This choice is made in view of numerical difficulties reported by Baker [9]. A detailed explanation is given in the paper by Baron *et al.* [10]. Furthermore, for a qualitative comparison of the temperature field with that from experiments, experimental data were measured using a laser interferometric technique. It is recognized that the realistic situation of the present problem is bound to exhibit a certain degree of unsteadiness as Reynolds number increases. The experimental results will be helpful in this regard to provide this bifurcation.

MATHEMATICAL FORMULATION

Differential equations

In this study, the two-dimensional, steady (for the cases studied which will be evidenced by experiments), laminar incompressible Navier–Stokes equations are solved numerically in terms of vorticity ω and stream function ψ. The false transient stream function is written as

$$\frac{\partial \psi}{\partial t} = \frac{\partial^2 \psi}{\partial x^2} + \frac{\partial^2 \psi}{\partial y^2} + \omega \tag{1}$$

and the conservation equation for the vorticity and temperature is

$$\frac{\partial \omega}{\partial t} + u\frac{\partial \omega}{\partial x} + v\frac{\partial \omega}{\partial y} = \frac{1}{Re}\left(\frac{\partial^2 \omega}{\partial x^2} + \frac{\partial^2 \omega}{\partial y^2}\right) \tag{2}$$

$$\frac{\partial \theta}{\partial t} + u\frac{\partial \theta}{\partial x} + v\frac{\partial \theta}{\partial y} = \frac{1}{Re\,Pr}\left(\frac{\partial^2 \theta}{\partial x^2} + \frac{\partial^2 \theta}{\partial y^2}\right). \tag{3}$$

Equations (1)–(3) are given in dimensionless forms. The normalizing factors for length, velocity and time are the height of the rib, s, the uniform approaching velocity, U_0, and s/U_0. The velocity is related to the stream function by

$$u = \frac{\partial \psi}{\partial y}, \quad v = -\frac{\partial \psi}{\partial x} \tag{4}$$

and dimensionless temperature θ is defined by $\theta = (T-T_0)/(T_w-T_0)$.

The pressure gradients near the corners of the rib are great, the surface pressure is also solved by applying the non-slip boundary condition at the wall to the Navier–Stokes equations, which become

$$\frac{\partial \bar{p}}{\partial x} = -\frac{1}{Re}\frac{\partial \omega}{\partial y}, \quad \frac{\partial \bar{p}}{\partial y} = \frac{1}{Re}\frac{\partial \omega}{\partial x} \tag{5}$$

where $\bar{p} = (p-p_0)/\rho U_0^2$ is the dimensionless pressure.

Integrating equation (5) with respect to x and y gives

$$\bar{p} = -\frac{1}{Re}\int_{x_0}^{x} \frac{\partial \omega}{\partial y}\,dx + \bar{p}(x_0)$$

$$\bar{p} = \frac{1}{Re}\int_{y_0}^{y} \frac{\partial \omega}{\partial x}\,dy + \bar{p}(y_0) \tag{6}$$

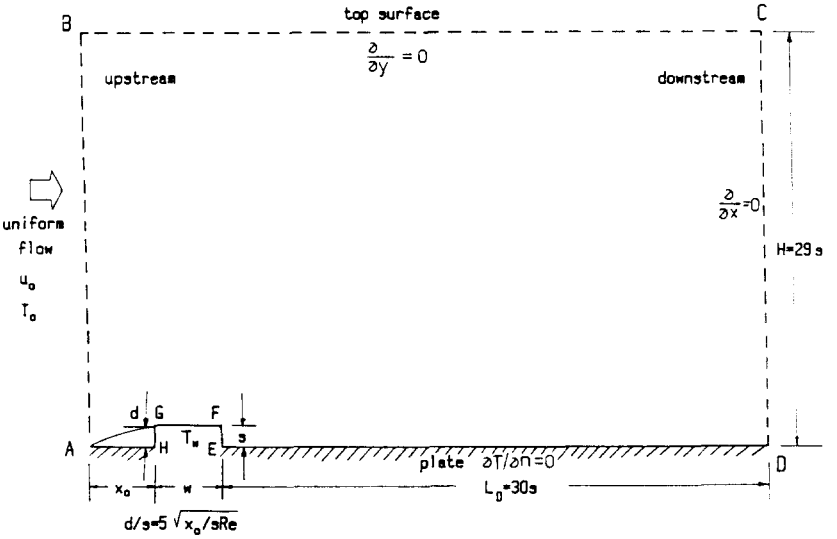

FIG. 1. Schematic of domain of calculations.

Boundary conditions

The boundary conditions are prescribed for the computational region indicated in Fig. 1. The approaching flow of uniform velocity U_0 is kept at the freestream temperature, T_0. The distance from the leading edge to the rib front face, x_0, is considered as a parameter in order to study the effect of the approaching boundary layer thickness on the separation regions; the approaching boundary layer thickness, d, is calculated from the relation for the laminar boundary layer on a flat plate

$$d/s = 5\sqrt{((x_0/s)/Re_s)}. \quad (7)$$

The downstream boundary is situated far away from the rib ($L_D = 30s$), so the property gradients along the streamwise direction can be considered to be negligible. The upper freestream surface is also far away from the plate ($H = 29s$), the region is sufficiently large to give computational results that are size independent. On the solid walls of the plate and rib, non-slip conditions apply. Table 1 summarizes the above descriptions of the boundary conditions and related geometrical parameters.

It is critical to approximate the boundary condition for vorticity at the solid wall. The gradients of pressure and vorticity in the vicinity of the rib are enormous. To avoid the numerical instability contributed by these great gradients, a method developed by Baron *et al.* [10] based on an accurate description of non-slip wall condition has been utilized.

Consider three grid points near the wall (see Fig. 2), the wall vorticity at a point close to the wall can be computed from the vorticity definition

$$\nabla^2\psi_2 = -\omega_2. \quad (8)$$

On the wall, the non-slip condition has to be satisfied, i.e. $(\partial\psi/\partial y)_1 = 0$

$$\left(\frac{\partial\psi}{\partial y}\right)_1 = \frac{1}{\alpha(1+\alpha)\Delta y}[\psi_1\alpha(2+\alpha)+\psi_2(1+\alpha)^2-\psi_3] + O(\Delta y)^2 = 0. \quad (9)$$

Table 1. Geometry parameters and boundary conditions

parameters	s	height of the rib, 1.27 cm
	w	width of the rib, 1.27, 2.54, 3.81, 5.08 cm
	H	$29s$
	L_D	$30s$
	x_0	1.9–29.3 cm
	top boundary	free
	d/s	0.4, 0.5, and 1.2
	w/s	1, 2, 3, and 4
	Re_s	200, 250, 300, and 400
boundary conditions	plate surface	$\psi = 0, \quad \omega = -\partial^2\psi/\partial y^2, \quad \partial\theta/\partial y = 0$
	rib surface	$\psi = 0, \quad \omega = -\partial^2\psi/\partial n^2, \quad \theta = 1$
	upstream	$\psi = y, \quad \omega = -\partial^2\psi/\partial x^2, \quad \theta = 0$
	downstream	$\partial^2\psi/\partial x^2 = 0, \quad \partial\omega/\partial x = 0, \quad \partial\theta/\partial x = 0$
	free surface	$\partial^2\psi/\partial y^2 = 0, \quad \omega = 0, \quad \partial\theta/\partial y = 0$

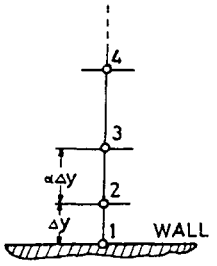

FIG. 2. Node details for the boundary.

Using equations (8) and (9), the computing process is as follows: ψ and ω of a point further from the wall than point 2 are calculated by iteration. The value of ψ_2 is obtained by solving equation (9) with ψ_1 given on the boundary and ψ_3 from the last iteration. Finally ω_2 is obtained from equation (8). In this process, no wall vorticity ω_1 is really needed.

NUMERICAL PROCEDURE

The system of governing differential equations with the boundary conditions is transformed to finite-difference equations by the control volume integration method with a power law scheme and solved by a procedure involving the ADI method and tri-diagonal matrix algorithm, with the wall stream function and vorticity boundary conditions given by equations (8) and (9).

The preassigned maximum residual value is 0.001 for all cases. The computational regions are decomposed by non-uniform grids of the finest grid of $0.02s$ adjacent to the wall, and the sizes of other grids are chosen such that each is within 125% of the next grid in order to avoid abrupt changes and to obtain convergence. Grid size dependence was examined and the final grid size (85×60) selected.

In the present algorithm, the ADI scheme is applied for obtaining convergence of each variable. The variable ϕ is said to be convergent if its residual is smaller than a preassigned value. The residual is defined as

$$\beta = \left| \frac{\phi_{i,j}^{n+1} - \phi_{i,j}^{n}}{\phi_{i,j}^{n}} \right|_{\max} \qquad (10)$$

where n refers to the nth iteration and i, j stands for the node position. In the above expression, the residual β represents the maximum value throughout the computational region. The preassigned maximum residual value is 0.001 for all cases. It was found that the first guess of the flow field is not essentially important as described in the literature. The relaxation parameters were set to 0.3 and the false time increment to 0.52. No internal iterations were performed. The present numerical calculation was performed on a CDC Cyber 840A at the Computer Center of the National Sun Yat-Sen University.

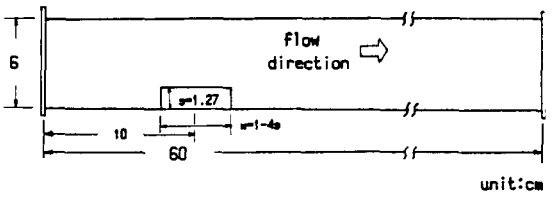

(a)

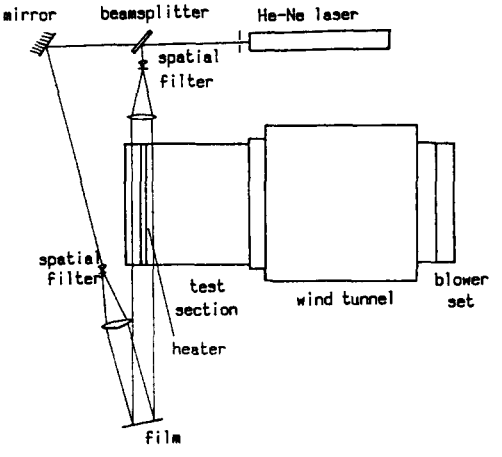

(b)

FIG. 3. Schematics of the experimental rig: (a) test section; (b) laser interferometric optical path.

EXPERIMENTAL RIG SETUP

In the present study, heat transfer information was obtained in a low speed wind tunnel by means of a laser interferometric technique. The wind tunnel, shown schematically in Fig. 3(a), is 1.5 m in length and is rectangular in cross-section with a working area at the test section of 60 cm width × 6 cm height × 60 cm length. The suction fan is composed of eight computer cooling fans. Its speed is varied by means of a voltage regulator. Except for the test section, the remaining components of the wind tunnel are constructed of 0.30 cm thick sheet metal. All walls of the test section are made of 0.5 cm plexiglass.

The laser interferometric technique has been discussed in great detail in the literature and will not be further elaborated on. To ensure a steady-state condition, the test apparatus was then allowed to run for approximately 1 h. The interferometric fringe pattern in the present study is recorded on a high speed holographic film. A 0.001 s exposure time is used throughout the present experiments. The processed negative film is then constructed with the aid of a TV camera and monitor. The freestream velocity in the wind tunnel is measured with a hot-wire probe.

A 150-cm field-of-view, 30 mW He–Ne laser-stimulated, interferometer was used as the temperature field indicating instrument (see Fig. 3(b)). This, when employed in the infinite-fringe mode, produced dis-

tinctive interferograms which are isotherm maps of the air flow over the rib.

RESULTS AND DISCUSSION

The flow field and temperature distribution

Figure 4 shows the representative contour plots of the dimensionless stream function and the corresponding isovorticity line for the cases of $Re_s = 200$, $d/s = 0.4$ for $w/s = 1$–4. It is seen from the figure that the approaching flow is curved and packed near the protruding corner. We can treat the $\psi = 1.0 \times 10^{-4}$ streamline as the separating streamline, i.e. $\psi = 0$, the boundary of the separated flow region and the solid boundary. There are two or three separated flow regions in these four cases. Existing separated bubbles are upstream of the front surface, above the upper surface of the rib (exists for $w/s = 3$ and 4), of which both are of strength smaller than -1.0×10^{-4} (not shown here), and the one located downstream behind the rear surface is shown as dotted lines. As one can see, for streamlines of $\psi > 0.1$, they are slightly influenced by the rib, they rise when they flow over the rib, and flow smoothly away from the rib.

As mentioned in Milos and Acrivos [11], increasing Reynolds number means the velocity increases and it makes the separated flow regions expand and the separated flow strength stronger; increasing d/s means the boundary layer became thicker while the velocity became smaller in the vicinity of the rib so that it makes the separated flow region expand, but the strength of the streamline is small; and w/s is an important parameter to the shape of the separated

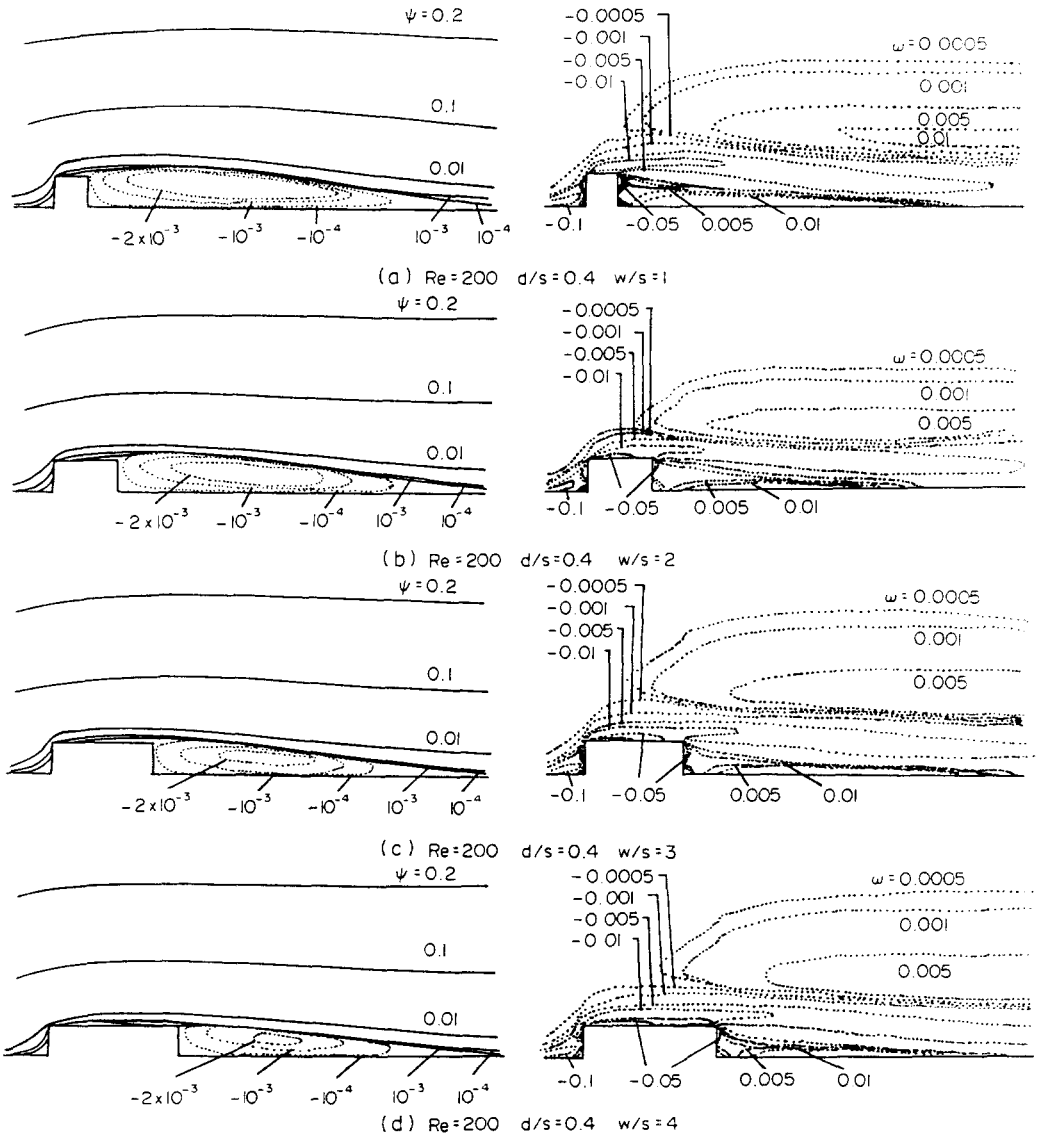

FIG. 4. Typical streamline and isovorticity line at $Re_s = 200$, $d/s = 0.4$, and $w/s = 1$–4.

flow region. These are also evidenced by the present results which are not shown here. Regarding the corresponding vorticity distribution (also shown in Fig. 4), it is seen that the vorticity which is very strong near the corners of the rib is swept and transported into the recirculation region. In addition, the decay of vortex strength in the transverse direction is rather fast compared with that in the streamwise direction. Within the recirculation regions, the value of the vorticity changes sign when one follows a closed streamline. The vorticity contours originated near upper corners of the rib for the up/downstream of the rib which agree well with those of previous studies for a backward facing step [12] and a forward facing step [10]. However, the influences of w/s on vorticity are not clearly noted. Moreover, it appears, for a fixed rib size, that an increase in Reynolds number would lead to an increase in the vortex strength (not shown here). This is because the Reynolds number increase designates an increase in the velocity which in turn increases a smaller initial boundary layer thickness at the rib. Thus, a smaller initial thickness gives rise to higher vorticity values in the separated region.

Figure 5 shows the corresponding dimensionless temperature distribution at $Re_s = 200$ and $d/s = 0.4$ for $w/s = 1$–4. The temperature contours are presented as dotted lines. As one can see, the temperature of the flow is influenced mainly in the vicinity and downstream of the rib. Upstream of the front surface of the rib, the temperature lines are packed close to the front surface near the protruding corner. For the lower position in the separated flow region, the temperature gradients are small, the temperature lines parallel to the front surface. It shows that in the separated flow region, the heat transfer is mainly by conduction, not by convection. Above the upper surface

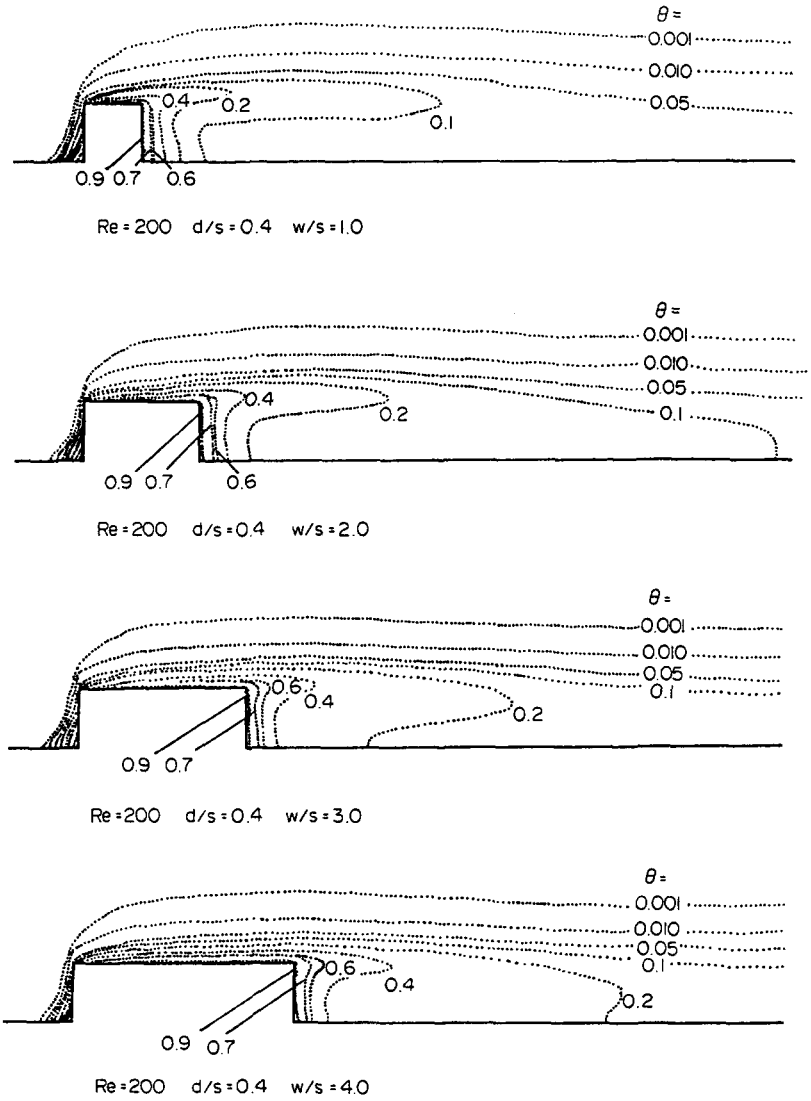

FIG. 5. Typical isothermal line at $Re_s = 200$, $d/s = 0.4$, and $w/s = 1$–4.

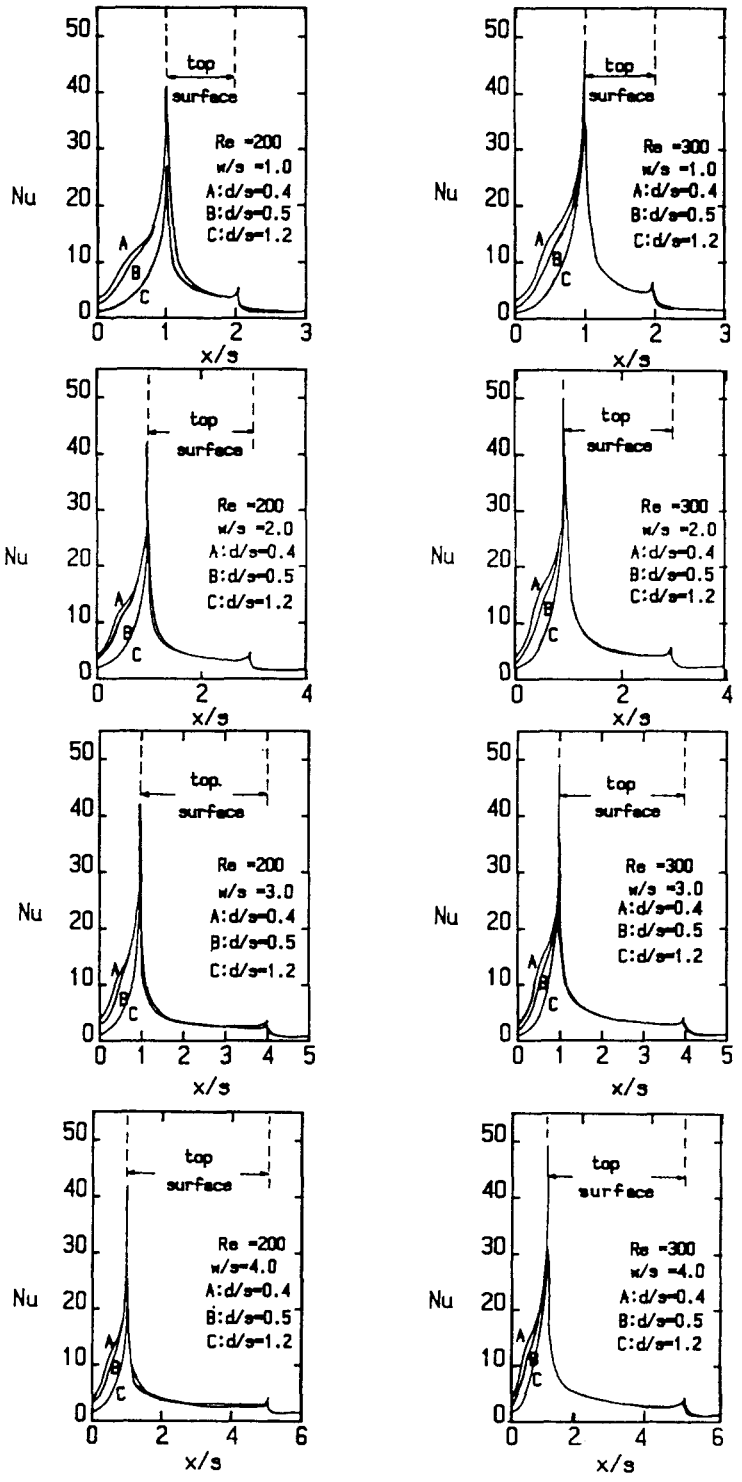

FIG. 6. Local Nusselt number distributions at $Re_s = 200$ and 300 for $w/s = 1$–4.

of the rib, the temperature lines pass through the region as the flow in the thermal developing region over a flat plate. These lines rise gently which results in the upper surface separated flow making no significant influence. In the reattached flow region, i.e. downstream of the rear surface, one can see from the temperature contour that the flow in the region flows in the clockwise direction; in the upper region, temperature lines are away from the rib, and, in the lower region, the temperature lines are parallel to the rear surface initially, and then are inclined to the rear surface a little prior to touching the wall. The temperature line $\theta = 1.0 \times 10^{-3}$ can be considered as the boundary of the thermal region influenced by the rib. The temperature contour downstream of the rib was affected more significantly than that of the upstream and upper surface of the rib as w/s varied.

Nusselt number distribution

Figure 6 shows typical variations of the local heat transfer on the side wall of the rib. The numerical results are expressed in the form of the Nusselt number. The local heat transfer was plotted against streamwise distance along the rib for $Re = 200$ and 300 at different w/s and d/s. For both cases the numerical data began from nearly zero from the lower corner where the temperature contours are further apart. Nusselt number increases fairly rapidly along the front face, giving the largest value at the end of the front face (the upstream protruding corner) at which the temperature contour lines are closely packed. Nusselt number then decreases mathematically until the flow reached or passed over the end of the top surface of the rib. At the downstream protruding corner the local heat transfer rises a little bit due to the cellular motion. Then, it decreases again prior to the region of the redevelopment of the boundary layer. In the upstream separated flow region, increasing Reynolds number makes the separated flow region expand, the temperature gradient decreased. For the upper part of the front surface outside the separated flow region, the velocity increases with increasing Reynolds number which results in a heat transfer rate increase. So is the upper surface of the rib. While, on the rear surface, the heat transfer rate is low and changes little when Reynolds number is varied. This fact can also be evidenced later in this section of Fig. 8.

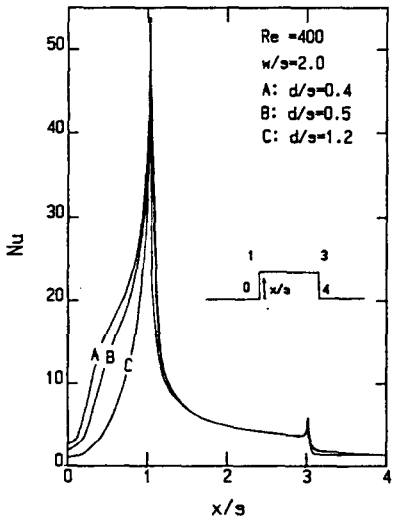

FIG. 7. Local Nusselt number distributions at $Re_s = 400$, $w/s = 2.0$ for $d/s = 0.4$, 0.5, and 1.2.

Table 2. Average Nusselt number of front surface, upper surface, rear surface, and entire surface of the rib for the cases studied

Re	d/s	w/s	$\overline{Nu}_f$	$\overline{Nu}_u$	$\overline{Nu}_r$	$\overline{Nu}_{av}$
200	0.4	1	12.600	7.507	1.871	7.326
		2	12.660	5.521	1.529	6.307
		3	12.660	4.706	1.352	5.626
		4	12.660	4.216	1.246	5.128
	0.5	1	11.310	7.341	1.730	6.749
		2	11.360	5.340	1.432	5.868
		3	11.360	4.474	1.264	5.210
		4	11.350	4.001	1.146	4.750
	1.2	1	5.990	5.990	1.369	4.450
		2	6.027	4.487	1.149	4.037
		3	6.022	3.768	1.015	3.668
		4	6.026	3.340	0.929	3.386
250	0.4	1	13.850	8.416	1.967	8.079
		2	13.870	6.081	1.632	6.917
		3	13.890	5.145	1.440	6.153
		4	13.880	4.599	1.347	5.603
	0.5	1	12.470	8.265	1.838	7.525
		2	12.500	5.936	1.524	6.474
		3	12.520	4.954	1.348	5.746
		4	12.510	4.410	1.243	5.233
	1.2	1	6.482	6.767	1.485	4.912
		2	6.514	5.030	1.264	4.460
		3	6.528	4.209	1.126	4.056
		4	6.515	3.736	1.018	3.746
300	0.4	1	14.890	9.153	2.051	8.700
		2	14.910	6.555	1.719	7.436
		3	14.920	5.489	1.515	6.581
		4	12.350	4.901	1.429	5.991
	0.5	1	12.390	8.621	1.901	7.624
		2	12.400	6.206	1.548	6.597
		3	12.420	5.160	1.424	5.860
		4	8.175	4.576	1.300	5.377
	1.2	1	8.175	7.956	1.643	5.925
		2	8.231	5.822	1.412	5.322
		3	8.236	4.842	1.251	4.803
		4	8.249	4.287	1.163	4.427
400	0.4	1	16.770	10.370	2.170	9.770
		2	16.790	7.337	1.849	8.328
		3	16.800	6.098	1.626	7.344
		4	16.790	5.428	1.535	6.672
	0.5	1	14.190	9.983	2.063	8.745
		2	14.240	7.082	1.748	7.538
		3	14.250	5.871	1.536	6.685
		4	14.250	5.203	1.453	6.087
	1.2	1	8.478	8.950	1.774	6.401
		2	8.522	6.525	1.529	5.775
		3	8.529	5.415	1.377	5.230
		4	8.528	4.788	1.282	4.827

Furthermore, a smaller approaching boundary layer thickness, in general, is shown to lead to higher vortices and hence to a higher heat transfer in the separated region, when the Reynolds number is held fixed and shear-layer thickness is allowed to change the dimension of the upstream plate, x_0. This can be evidenced by Fig. 7 for $d/s = 0.4$ having the highest value of local heat transfer rate all over the rib surface.

The effect of the aspect ratio of the rib w/s on local Nusselt number is shown in Fig. 8 at $d/s = 0.4$. Increasing w/s, the upper surface area increases and, consequently, the total heat transfer amount increases. The rear surface heat transfer rate decreases as w/s increases because of the more heated flow passed over the upper surface. As can be seen from Figs. 6–8, they give Nu results in the upper front corner of about 50 which is much larger than those of previous studies (see Hsieh and Huang [5] for surface-mounted ribs and Baron *et al.* [10] for forward-facing steps). This is partly due to the present study including the effect of boundary layer thickness and partly due to the present geometry being different from the results reported by Baron *et al.* even though they already considered the effect of approaching boundary layer thickness (d/s).

It is more practical for the average heat transfer rate over the surface of the rib than the local heat transfer rate. The average Nusselt numbers of the front face, upper surface, rear face and entire surface with the relationship of the relevant parameters are illustrated in Table 2. For instance, it is found that the variation of w/s does not affect the $\overline{Nu}_f$ but the values of $\overline{Nu}_u$ and $\overline{Nu}_r$ decrease as w/s increases.

With the values illustrated in Table 2, the overall average Nusselt number ($\overline{Nu}_{av}$) over the entire surface of the rib with parameters Re_s, w/s, and d/s was further correlated in the form of

$$\overline{Nu}_{av} = 0.44(Re_s)^{0.465}(d/s)^{-0.36}(w/s)^{-0.265}. \quad (11)$$

This correlation is shown in Figs. 9–11. Examining

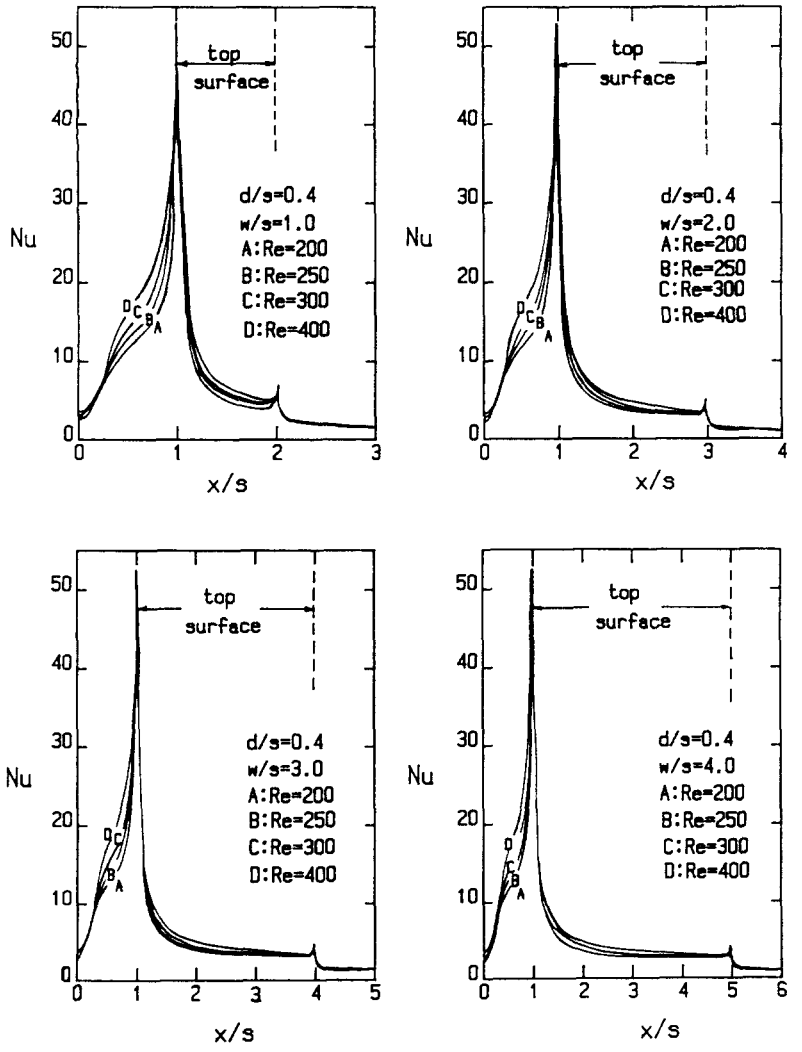

FIG. 8. Nusselt number distributions at $d/s = 0.4$, $w/s = 1$–4 for $Re_s = 200$, 250, 300, and 400.

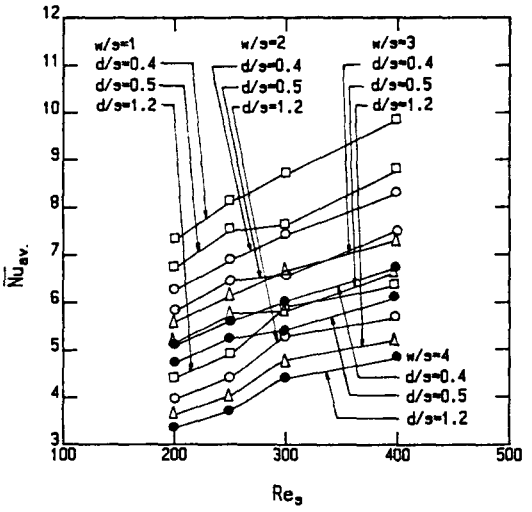

FIG. 9. $\overline{Nu}_{av}$ vs Re_s.

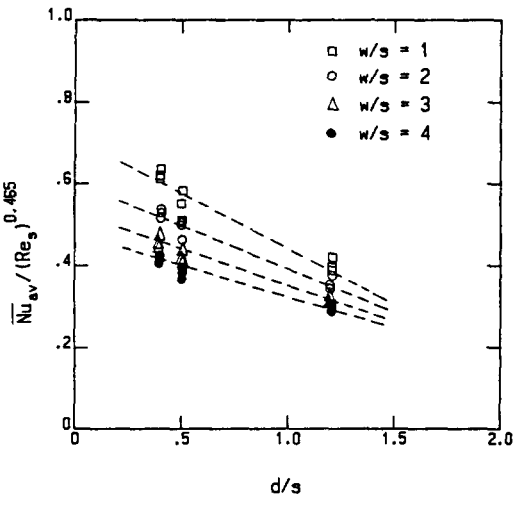

FIG. 10. $\overline{Nu}_{av}/Re_s^{0.465}$ vs d/s.

equation (11) with the numerical result, the maximum relative error is 10%, and the mean relative error is 2.7%. Nevertheless, the result seems acceptable. Figure 12 further shows the numerical results plotted against the data from the correlation. As expected, 90% of the predicted data is within a 45° diagonal band (45° ± 3°) which shows the present correlation would be good and useful.

In Fig. 13, comparison is made with the correlations developed by Hsieh and Huang [5] and Davalath [13] which can be considered as two limiting cases for the present study with the rib aspect ratio $w/s = 2$. For the correlation by Hsieh and Huang [5], the plate upstream of the rib is kept at the same temperature as the rib, the flow is heated by the plate before it approaches the rib, the heat transfer rate is hence reduced. For the correlation of Davalath [13] the plate is kept insulated, while the rib has a heat source uniformly distributed in the area of the rib so that the surface temperature gradient is lower which results in a higher heat transfer rate. This shows that the presented results exhibit a distribution in between these two limiting cases.

Comparison with experimental results

Figure 14 shows one of the interferograms of the temperature field for both the front and rear parts of the rib for the case of $Re_s = 300$, $d/s = 1.2$, $w/s = 3$, respectively. Upstream of the front surface of the rib, the constant temperature lines distribute the trend similar to those obtained from the numerical results. Over the upper surface, the temperature lines develop

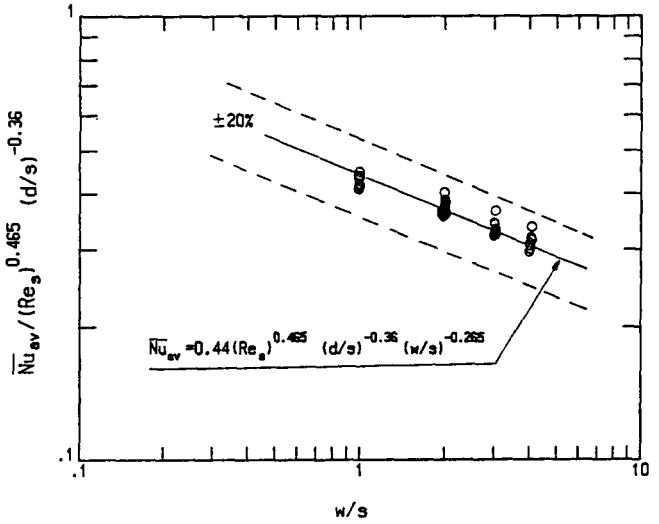

FIG. 11. Correlation of $\overline{Nu}_{av}$ with Re_s, d/s, and w/s.

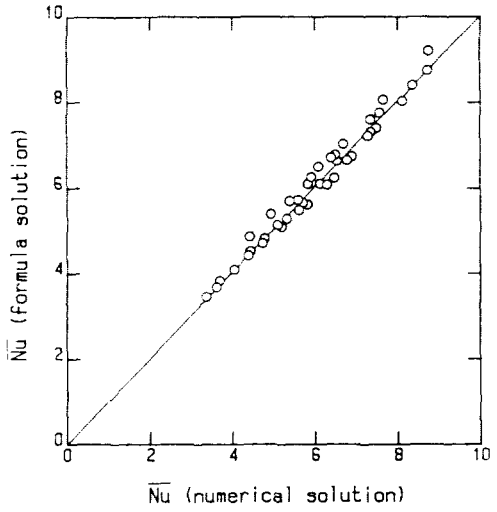

FIG. 12. Performance plot of the correlation.

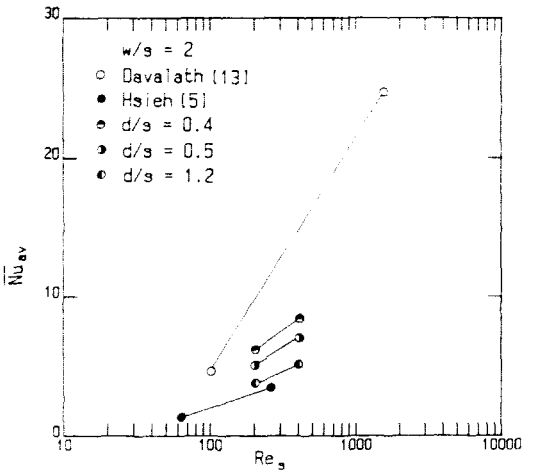

FIG. 13. $\overline{Nu}_{av}$ vs Re_s for $w/s = 2$ and comparison with Davalath [13] and Hsieh and Huang [5]

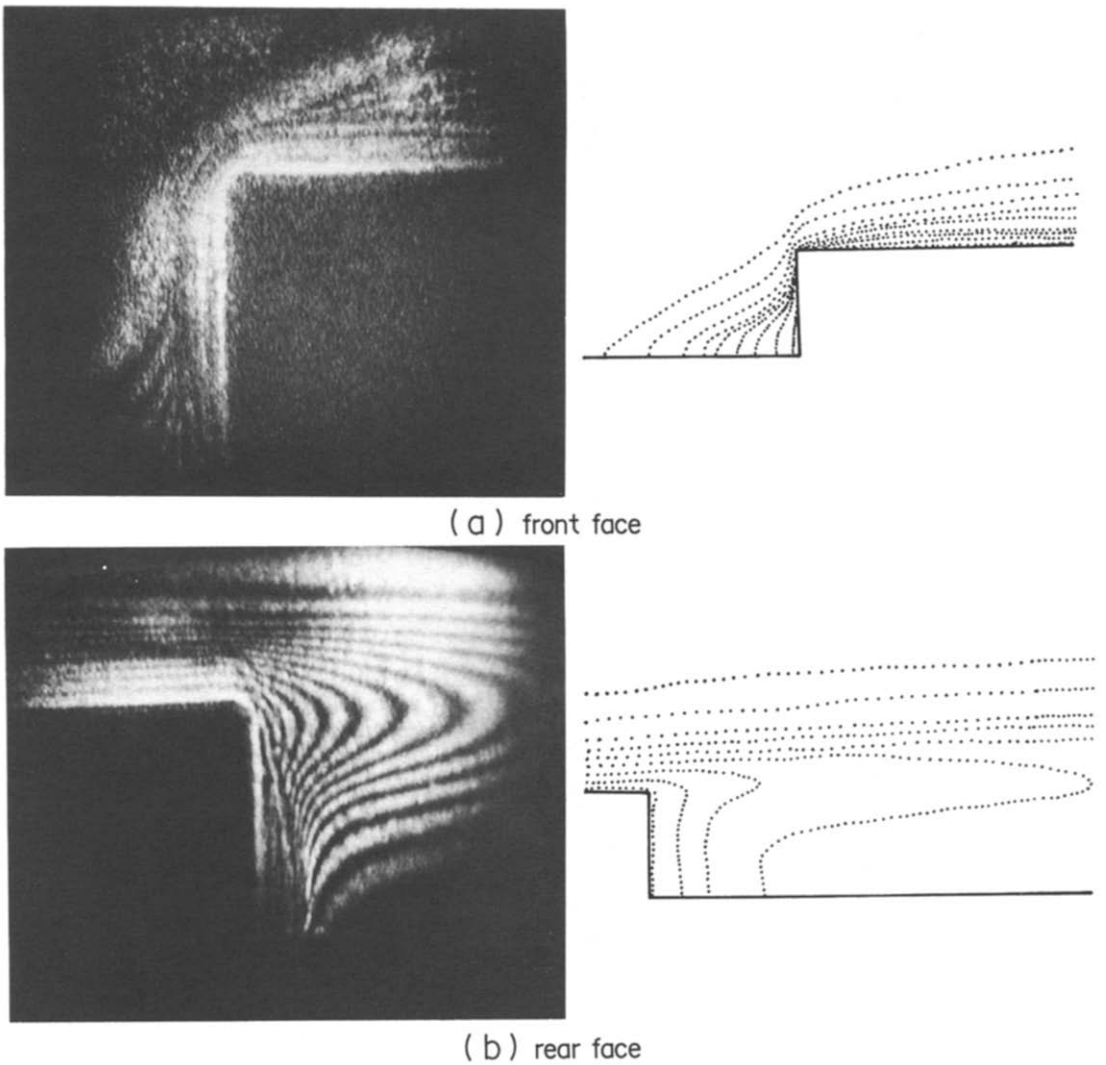

FIG. 14. Comparison of the numerical results (right) with those of experiments (left) at $Re_s = 300$, $d/s = 1.2$, and $w/s = 3$.

in such a way as the thermal developing flow for the flat plate flow. In addition, one can see that the temperature lines change direction backward in the boundary region of the reattached flow, finally, packed to and parallel to the rear surface. This agrees reasonably well with those from the numerical results also shown on the right-hand side of Fig. 10 for the same tendency of the temperature distributions. The steadiness of the flow was examined to assess the previous steady state assumption of the present numerical calculations. It was found that the flow would suffer the unsteadiness when $Re_s > 400$. Since the image processing system is not available to the authors at this stage, it is not easy to get quantitative information from the present interferograms.

CONCLUSION

In the present study, the effects of Reynolds number, initial boundary layer thickness, and aspect ratio (width-to-height ratio) of the rib for the heat transfer coefficients are discussed. Increasing Reynolds number increases the heat transfer rate because of the increasing flow velocity. For the same reason, a small d/s has a higher heat transfer coefficient because for a large d/s, the rib is immersed in the boundary layer resulting in less influence to the flow. Increasing w/s decreases the average heat transfer rate over the upper surface but increases the total heat transfer rate by increasing the surface area.

Overall the average Nusselt number correlation over the entire surface of the rib is made for parameters Re_s, d/s and w/s, and compared with two limiting cases of the previous studies. The deviation is reasonable.

Moreover, the numerical temperature distribution is compared qualitatively with the interferometric experimental result. It is found that the agreement is fairly good.

Acknowledgement—Partial financial support from the National Science Council, Taiwan, Republic of China, under Grant No. NSC-78-0401-E110-07, is greatly appreciated.

REFERENCES

1. M. L. Buller and R. F. Kilburn, Evaluation of surface heat transfer coefficients for electronic module packages, Heat Transfer in Electronic Equipment, HTD, ASME Winter Annual Meeting, Vol. 20, pp. 15–20 (1981).
2. R. A. Wirtz and D. Dykshoorn, Heat transfer from arrays of flat packs in a channel flow, *Proc. 4th Int. Electronics Packaging Soc.*, Baltimore, Maryland, pp. 318–326 (1987).
3. S. S. Hsieh, Thermal characteristics of annular flow with asymmetrically roughened surfaces, *Int. J. Heat Fluid Flow* **9**, 78–82 (1988).
4. S. S. Hsieh and D. Y. Huang, Flow characteristics of laminar separation on surface-mounted ribs, *AIAA J.* **25**, 819–823 (1987).
5. S. S. Hsieh and D. Y. Huang, Numerical computation of laminar separated forced convection on surface-mounted ribs, *Numer. Heat Transfer* **12**, 335–348 (1987).
6. W. Aung, An interferometric investigation of separated forced convection in laminar flow past cavities, *ASME J. Heat Transfer* **105**, 505–512 (1983).
7. D. R. Chapman, A theoretical analysis of heat transfer in regions of separated flow, NACA TN 3792 (1956).
8. A. Bhatti and W. Aung, Finite difference analysis of laminar separated forced convection in cavities, *J. Heat Transfer* **106**, 49–54 (1984).
9. S. Baker, Regions of recirculating flow associated with two-dimensional steps, Ph.D. Thesis, University of Surrey (1977).
10. A. Baron, F. K. Tsou and W. Aung, Flow field and heat transfer associated with laminar flow over a forward-facing step, The 8th Int. Heat Transfer Conf., San Francisco, pp. 22–29 (1986).
11. F. S. Milos and A. Acrivos, Steady flow past sudden expansions at large Reynolds number—II. Navier–Stokes solutions for the cascade expansion, *Physics Fluids* **30**, 7–18 (1987).
12. W. Aung, A. Baron and F. K. Tsou, Wall independency and effect of initial shear-layer thickness in separation flow and heat transfer, *Int. J. Heat Mass Transfer* **28**, 1757–1770 (1985).
13. J. Davalath and Y. Bayazitoglu, Forced cooling across rectangular blocks, *ASME J. Heat Transfer* **109**, 321–328 (1987).

CONVECTION FORCEE LAMINAIRE A PARTIR DE NERVURES MONTEES SUR DES SURFACES

Résumé—On présente une étude numérique et expérimentale sur le transfert thermique par convection forcée à faible vitesse autour de nervures transversales bidimensionnelles dont les parois sont à température uniforme. Les effets du rapport de forme et du nombre de Reynolds ainsi que de l'épaisseur initiale de la couche limite sont analysés et discutés. La technique numérique est basée sur une loi puissance combinée avec une fausse forme de fonction de courant–vorticité. On trouve que les valeurs des températures s'accordent raisonnablement bien avec celles tirées des expériences. Les résultats sont corrélés sous forme de l'équation

$$\overline{Nu}_{av} = 0{,}44(Re_s)^{0.465}(d/s)^{-0.36}(w/s)^{0.265}.$$

LAMINARE ERZWUNGENE KONVEKTION AN BERIPPTEN OBERFLÄCHEN

Zusammenfassung—Der Wärmeübergang durch erzwungene Konvektion bei kleinen Strömungsgeschwindigkeiten wird numerisch und experimentell an zweidimensionalen Querrippen untersucht, wobei die Grundfläche auf konstanter Temperatur gehalten wird. Die Einflüsse des Abmessungsverhältnisses und der Reynolds-Zahl sowie der anfänglichen Grenzschichtdicke werden ermittelt und diskutiert. Das numerische Verfahren beruht auf einem Potenzansatz in Kombination mit einer "falschen" Stromfunktion-Wirbelintensität-Formulierung. Es zeigt sich, daß die berechneten Temperaturen befriedigend mit Meßwerten übereinstimmen. Die Ergebnisse werden schließlich mit einer Gleichung der folgenden Form korreliert:

$$\overline{Nu}_{av} = 0.44(Re_s)^{0.465}(d/s)^{-0.36}(w/s)^{-0.265}.$$

ЛАМИНАРНАЯ ВЫНУЖДЕННАЯ КОНВЕКЦИЯ ОТ РЕБЕР, РАСПОЛОЖЕННЫХ НА ПОВЕРХНОСТИ

Аннотация—Численно и экспериментально исследуется слабоинтенсивный вынужденноконвективный теплоперенос у двумерных поперечных ребер с однородной температурой стенок. Анализируется роль отношения сторон, числа Рейнольдса, а также начальной толщины пограничного слоя. Численная методика основана на степенном законе в сочетании с использованием квазифункции тока-завихренности. Установлено, что численные данные по температуре качественно хорошо согласуются с результатами экспериментов. Результаты обобщены в виде следующей критериальной зависимости

$$\overline{Nu}_{av} = 0.44(Re_s)^{0.465}(d/s)^{-0.36}(w/s)^{-0.265}.$$